

# Fine modulations in the diffraction pattern of boron nitride nanotubes synthesised by non-ablative laser heating

T. Laude<sup>a</sup> and Y. Matsui

National Institute for Materials Science, Advanced Materials Laboratories, Namiki 1-1, Tsukuba, Ibaraki, 305-0044, Japan

Received: 31 May 2002 / Received in final form: 27 May 2004 / Accepted: 15 June 2004  
Published online: 30 August 2004 – © EDP Sciences

**Abstract.** Non-ablative laser heating has recently turned out to be an efficient synthesis method for boron nitride (BN) nanotubes, offering flexibility in the control of experimental parameters. Long tubes are obtained as a hairy growth on the target around laser impact. Tubes are mostly assembled in bundles and thin. Selected area diffraction diagrams reveal that zigzag and armchair helicities are dominant, without preference. A field emission gun enabled to resolve the fine modulations in the diffraction diagrams for multi-walled nanotubes (MWNT) and for bundles of MWNT. The interpretation of the diffraction pattern of nanotubes is generalised for such modulations, considering the analytical expression of the diffracted amplitude at each graphite reflection. The fine modulations in the pattern are linked to roll diameters, bundle lattice, and interlayer distances. Experimentally, several roll diameter modulations are observed. Unusual modulations corresponding to an interlayer distance of 2 layers are also observed. They show a two-roll period, with an alternative shift along tube axis, in the piling of the rolls of MWNT.

**PACS.** 61.46.+w Nanoscale materials: clusters, nanoparticles, nanotubes, and nanocrystals – 81.07.De Nanotubes – 68.37.Lp Transmission electron microscopy (TEM) (including STEM, HRTEM, etc.)

## 1 Introduction

Crystalline tubes of nanometre dimensions, “nanotubes”, are known since the development of high-resolution microscopy. (See [1] for instance.) In the last ten years, much effort has been invested to enable their usage in nano-technologies and nano-materials. Boron nitride (BN) nanotubes are a promising candidate for high temperature applications, where the reactive character of carbon is cumbersome. Indeed, the ionic character of the BN bounding makes it extremely stable, especially towards oxidation, molten metals or silicon [2, 3].

Recently, we showed that a non-ablative laser heating method could produce very long BN nanotubes assembled in bundles [4]. A CO<sub>2</sub> laser beam, both continuous and low power, was focused on a surface of condensed BN powders, and induced a stable local heating. A macroscopic growth of nanotubes was found on target front surface. The mass of nanotubes formed a crown rising perpendicularly from surface (Fig. 1a), on a ring around impact, where the range of surface temperatures is such that boron is liquid [5].

To determine the regularity of crystalline characteristics of the product, such as the diameter of bundles/tubes, the helicity of tubes, the ordering of tubes inside a bundle (...), the combination of transmission electron microscopy (TEM) imaging and selected area diffraction (SAD) is of prime importance. Here, we present the re-

sults obtained using such techniques. We will show that TEM imaging of long BN fibres meets some limitations, firstly caused by electron charging of BN structures under the beam. We show that, nevertheless, the SAD technique can give useful complementary information. We present a practical way to interpret the diagrams and apply it to ours, obtained with a fine resolution thanks to the use of a field emission gun (FEG).

## 2 Synthesis method and observations at low magnification

Details of the synthesis method have been given elsewhere [5] and are repeated here only for convenience. We used a continuous CO<sub>2</sub> laser beam, 70 W, quasi monochromatic at  $\lambda = 10.6 \mu\text{m}$ . The target was a cube ( $\sim 4 \text{ mm}$ ) of commercially available h-BN. It was introduced into a vacuum chamber, on the top of a h-BN stand, first at a position such that the laser beam was over-focused. The chamber was pumped to a secondary vacuum and the laser was switched on. In such conditions, the target was not degraded by dissociation and could be roughly out-gazed for 5 min. After cooling down, the target was irradiated a second time, but for  $\sim 5 \text{ s}$ . Then, the target that moved (after opening and re-pumping) at laser waist. Finally, the

---

<sup>a</sup> e-mail: thomaslaude@yahoo.fr

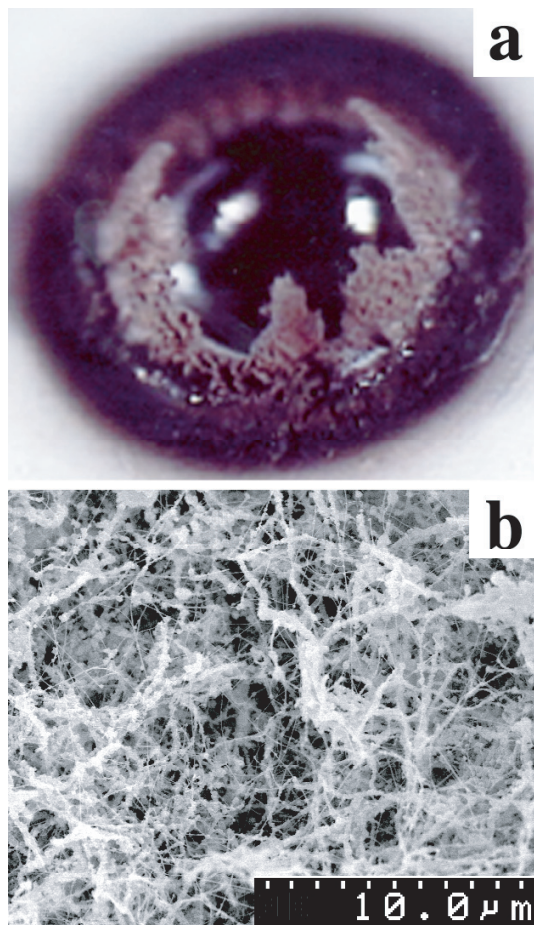


**Fig. 1.** (a) Growth around laser impact (binocular microscope image). The cavity ( $\sim 0.5$  mm) is partly filled with drops of solidified boron. On a ring ( $\sim 0.12$  mm thick) around cavity, BN nanotubes (in bundles) grow mixed with nano-particles powders, forming a crown rising perpendicular to target surface. Further away, the surface is covered by a deposit of boron rich nano-particles. Diameter of the three zones is  $\sim 1$  mm. (b) A scanning electron microscope (SEM) image of the crown material. Long nanotubes are mixed with nano-particle powders.

chamber was filled with nitrogen at 100 mbar and, the target was heated on  $\sim 100$   $\mu\text{m}$ , for several minutes. At the end of the experiment, the apparatus was left to cool down  $\sim 5$  min before opening to air, to avoid an eventual oxidation.

Under the beam, dissociation is induced locally and a cavity is formed on the target. (See Fig. 1a). Nitrogen effuses as a gas. Boron is partly left as liquid drops in the cavity and partly evaporated. In the first 15 seconds of the heating, evaporated boron spreads on target, around cavity, as boron rich nano-particles. On a specific ring around cavity, where temperatures of the target are in the range of liquid boron, these particles develop into BN nanotubes. The mass of tubes forms a hairy growth around impact in the shape of a crown.

At low magnification (Fig. 1b), material from the crown appears as a mix of fibres (bundles of tubes or in-

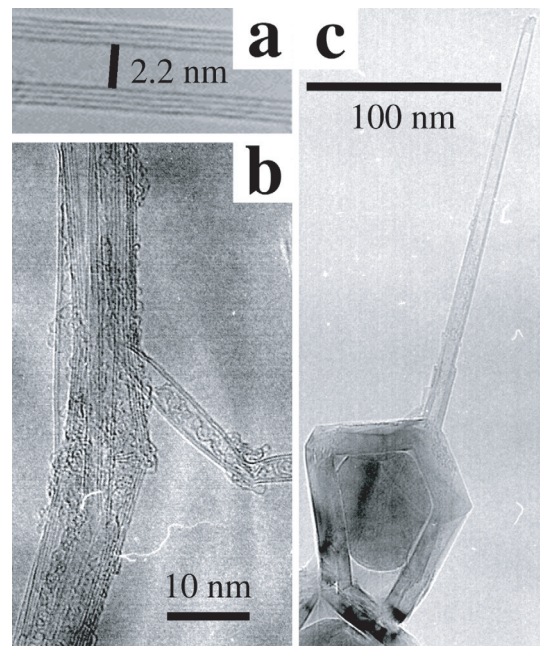


**Fig. 2.** Transmission electron microscope (TEM) imaging of BN tubes. (a) A 4-layer BN tube. (b) Lateral image of a thin bundle. (c) Tube emerging from a “seeding” BN nano-particle containing a boron core. Note that the boron core is on the same side than tube root (it could have fed the growth), and that there is a separation tube/seed through a large BN wall (it could have stopped the growth).

dividual tubes) and nano-spherical particles (BN onions often containing a boron core), which readily adhere to each other through weak interactions, or by structural merging. Nano-particles are often present at tube extremities (Fig. 2c), indicating that nano-particles nucleate the growth of tubes. It is not clear if tube growth occurs only at target surface, or also up-crown, away from target surface.

With scanning electron microscope (SEM) imaging, fibres are observed very long and entangled, and form tissue-like texture. Although a measurement of the average length is not possible, fibres are typically discerned from the rest of the material on several tens of microns, between knots. The longest piece observed was 120  $\mu\text{m}$ , and was obtained for the longest duration experiment (12 min), suggesting that tubes grow continuously during the whole experiment.

### 3 High resolution TEM study

#### 3.1 Technique and limitations

TEM observations were mainly performed on a Hitachi HF-3000 operating at 300 kV and equipped with a FEG gun. Powders for observation were collected manually on target surface with small tweezers, and deposited

on a carbon micro-grid supported by a copper grid. Observations were mostly undertaken on the holes of the carbon micro-grid. Because fibres are highly entangled, they have a poor ability to spread on the micro-grid. (Adding drops of solvent brings little improvement.) However a representative fraction of the product is thin enough to transmit the electron beam and allows imaging. The main drawback for imaging is the fact that BN structures are electrically resistant and hence, accumulate charges. Under the beam, most of the product is subject to micro movements. Observation is possible in regions with close links to the carbon grid but still, images may be blurred by nano-vibrations and drifts. This problem is critical at high resolution, because of the higher density of the beam.

In some cases, vibrations of an angstrom order may lead to confusing images. Especially, a double-wall tube may appear to have single-wall-like fringes (white/black modulation on one wall) in some regions, and show double-wall-like fringes only in stable regions. To determine the presence of a single-walled nanotube (SWNT), the thickness at mean contrast of one wall should be close to the resolution of the microscope ( $\sim 2 \text{ \AA}$ ). On the other hand, if the thickness is of the order of interlayer distance + resolution ( $\sim 5 \text{ \AA}$ ), the tube may be double-walled.

High-resolution imaging is best realised in a region with close contacts to the micro-grid. One reason is that it is mechanically stable because the product has less amplitude for vibrating. Another reason is that the local charge is more easily evacuated. For instance, it is usually better to observe the smallest agglomerations of product. Those have closer contacts to the supporting carbon layer. Contacts are especially critical when observing long fibres, because they are separated from the supporting carbon layer on long distances. Fibres are unstable and charges have to travel along a significant distance before escaping to the supporting carbon layer. Most of all, the electron beam affects fibre extremities which are free standing.

Several precautions may lower charging effect. It is often worth limiting the illuminated zone to the structures observed. The beam collected by the material out of the observing area contributes to the global charging effect. For this, we select a small condenser aperture and condense the illumination beam. It was found that charging effect is sensibly lower at 800 kV in a Hitachi 1500 microscope. Lowering the accelerating voltage to 100 kV was not found helpful. Attention should be paid to the fact that the illumination beam sensibly affects the position of structures, hence the focus.

### 3.2 Experimental observations at high resolution

See Figure 2. TEM observations reveal that most fibres are BN nano-tubes self-assembled in bundles. A bundle contains a few tubes, up to several tens. Bundles are often branched along their length, one or several tubes diverging from the main bundle. Under intense electron irradiation, bundle extremities tend to split into their constituent tubes, forming a brush like extremity, and attesting for the weakness of the inter-tube bounding. (In these conditions,

tubes are also damaged and shortened by ejection of their constituent atoms.)

Internal tubes can be observed when imaging a thin bundle laterally (Fig. 2b). Larger bundles usually appear as uniform ribbons without contrast. Tubes can also be discerned in the section of a bundle, however such imaging is made difficult by the charging effect. (When imaging, the electron beam should be in the plane formed by a loop of a bundle, and this is typically an unstable configuration.) Because of this limitation, an eventual 2D-triangular lattice inside the bundle could not be evidenced. (A X-ray study could be better suited, but this requires a quantity of product higher than presently available.)

Individual tubes can be imaged at high resolution if they are away from a bundle, or inside a thin bundle. Most tubes are very thin (typically 2, 3 or 4 layers). SWNT were not evidenced (with the criteria mentioned above or with diffraction). High resolution could neither give evidence that double-walled tubes are dominant inside bundles (as mentioned in other reports). Tube diameters are remarkably constant along tube axis. The inner diameter is often close to 2 nm, which is also a minimum value. This is probably due to a constraint specific to multi-walled BN tubes: a strong curvature is structurally costly for the inter-layer accommodation. Exceptionally, the section of an individual tube could be imaged by TEM [4]. The section is circular (and not polygonal), but does not allow a firm confirmation that layers are concentric and not spiralling in the tube.

Apart from bundles, various individual tubular morphologies are also observed. Such tubes are often thick (typically, ten layers), and very straight (little flexible). Their diameter may be irregular, with steps or with a continuous thickening along axis. A few fibres may be spiralling, but this may result as well from a mechanical torsion around axis than from a specific structure. The flexibility of thin tubes is evidenced by their ability to curve under the beam when charged.

Some amorphous material may be present on, or rarely in, tubes cylinder, possibly amorphous boron, or carbon contamination from the TEM. In addition, spherical particles tend to agglutinate along fibres, merging to each other and to fibres. Their constituent atoms sometime appear to have diffused along the fibre axis for hundreds of nanometre, sometime forming an irregular shell of h-BN layers parallel to fibre surface.

### 4 Selected area diffraction (SAD) study

The interpretation of the pattern is the same for BN and carbon fibres, due to the same hexagonal lattice and to the very close form factor of B/C/N atoms. We suppose beam axis perpendicular to fibre axis ( $z$ -axis).  $r$ -axis is perpendicular those two axis. These notations are used indifferently for real and reciprocal space.

#### 4.1 Diffraction pattern expected from tubes and bundles

Nanotube pattern can be indexed by graphite reflections [6–9] as 002i reflections on  $r$ -axis due to hexagonal planes parallel to the beam (characteristic of multi-layering), and  $gh0$  (mainly 100 and 110) reflections due to planes perpendicular to beam axis (characteristic of helicities). The number of helicities observed is usually lower than the number of rolls in one tube because several rolls share same helicity. (And some helicities may not be observable.) This is especially true if the interlayer accommodation tends to respect  $h$ -BN piling. Pattern intensity does not obviously give an indication of the number of layers diffracting because of interferences. Hexagons neither parallel nor perpendicular to beam axis are responsible for a continuous streaking of the reflections, perpendicular to  $z$ -axis and away from it, affecting in particular reflections at low angle to  $z$ -axis.

##### 4.1.1 Modulations in the pattern of a SWNT

The diffraction pattern from a SWNT is a finite number of lines perpendicular to  $z$ -axis and spaced by  $1/C$ , where  $C$  is the true period along the tube. The intensity of each line can be expressed as a sum of Bessel functions: [10–12]

$$F(R, \Phi = 0, l) = \sum_n F_n(R, l),$$

with

$$F_n(R, l) = \exp \left[ in \left( \frac{\pi}{2} \right) \right] J_n(2\pi r_0 R) \times \sum_j f_j \exp \left[ i \left( n\phi_j + 2\pi \frac{lz_j}{C} \right) \right]. \quad (1)$$

We use notations of [10].  $R$  and  $\Phi$  are the cylindrical coordinates in the reciprocal space; (we imposed  $\Phi = 0$  in the observation plane)  $l$  is line number along  $z$ -axis.  $r_0$  is tube radius and the last sum is done over all atoms in the true cell.

However, practically, the sum over  $n$  can be limited to a few terms:  $J_n(x)$  reaches first maximum near  $x = \pm n$  (verifiable numerically). Hence for a given  $R$ , term(s)  $n \sim 2\pi r_0 R$  is (are) dominant. In addition, for  $n \sim 2\pi r_0 R$  the atomistic sum on  $j$ , approaches standard graphite reflections. ( $J_n$  may cause a position shift along  $l$  line.) Hence, practically, near-graphite reflections are observed. ( $l$  lines that do not approach any low angle graphite reflection will be not observed.) We may write near such reflections,  $F(R, l) \sim F_{n \sim 2\pi r_0 R}(R, l)$ , and index them by  $(n, l)$  (as well as by  $gh0$ ).

$J_n(x)$  is roughly modulated with a period  $2\pi$  near first maximum. Hence, reflections are modulated (in intensity) along the  $l$  line, and their modulation is directly related to roll diameter as  $\Delta R \sim 1/(2r_0)$ . Roll diameter modulation (RDM) were observed experimentally for

carbon SWNT [13] and for BN tubes [5]. All  $gh0$  reflections may have a RDM (and not only the 000 reflection). As  $J_n(x)$  period increases with  $n$ , RDM period increases slowly with  $n$ . For instance, at a distance from  $z$ -axis corresponding to the 100 reflection of graphite ( $R \sim 4.7 \text{ nm}^{-1}$ ), and considering a  $r_0 = 1 \text{ nm}$  tube, the typical Bessel order is  $n \sim 30$  and the period of the RDM is increased by a factor  $\alpha \sim 1.9$ . At a distance corresponding to the 110 reflection of graphite ( $R \sim 8.1 \text{ nm}^{-1}$ ),  $n \sim 50$  and the period is increased by a factor  $\alpha \sim 2.2$ . ( $\alpha$  is found numerically.)

##### 4.1.2 Modulations in the pattern of a bundle of SWNT

A regular lattice of identical SWNT (indexed by  $m$  and at abscise  $r_m$ ) only disordered along  $z$  (by  $z_m$ ), and around their axis (by  $\phi_m$ ) diffracts at one reflection  $(n, l)$  the amplitude: [10]

$$F_n(R, l) \sum_m \exp[i(r_m R - \delta_{m,l})] \quad \text{where} \quad \delta_{m,l} = 2\pi l \frac{z_m}{C} + n\phi_m. \quad (3)$$

Hence, the diffracted pattern is the product of previous SWNT term (giving the RDM), with a lattice factor. When the number of tubes is large, the first term in the exponential potentially causes bundle lattice modulation (BLM), allowing a collection of line parallel to  $z$ -axis, with a periodicity depending on the orientation of the beam. For numerical modelisations of BLM see [12, 14, 15].

However, BLM are hidden by the random term  $\delta_{m,l}$  for most of the reciprocal space. At 000 ( $l$  and  $n = 0$ ) BLM is observable because  $\delta_{m,l} = 0$ . But, if variations of  $\delta_{m,l}$  are such that  $|\delta_{m,l}| > \pi$ , BLM are not observable. Considering that  $z_m$  and  $\phi_m$  are roughly limited to respectively,  $a$  (cell dimension) and  $a/r_0$ , the zone where BLM may be observed is roughly the centre of the reciprocal space, limited at  $l_{max} = C/(2a)$  on  $z$ -axis and at  $n_{max} = (\pi r_0)/a$  on  $r$ -axis, hence where  $|R_{max}| < 1/(2a)$ . Therefore, such BLM should only be observed near 000.

In addition, BLM does not appear if the bundle is thin (broadening by bundle thinness), or if the position of the tubes is irregular in the bundle (broadening by the typical disorder distance). Hence, BLM are rarely observable. If BLM did appear, it may mix with RDM, which has the same order of periodicity, making the diagram locally difficult to interpret.

##### 4.1.3 Modulations in the pattern of a MWNT

If rolls of a MWNT have different helicities, their patterns mostly do not superpose (except at 000), and the interpretation of the diffraction is straightforward. If rolls have same helicity, patterns superpose at each reflection. We can suppose that the rolls are only disordered along

and around  $z$ -axis. Then, the diffracted amplitude of one roll  $m$  at one reflection is:

$$F_n^m(R, l) \sim \exp \left[ in \left( \frac{\pi}{2} \right) \right] J_n(2\pi r_{0,m} R) \times \sum_{j_m} f_{j_m} \exp \left[ i \left( n(\phi_{j_m}) + 2\pi \frac{l(z_{j_m})}{C} \right) \right]. \quad (4)$$

The total amplitude at one reflection is found by summing such term for each roll contributing. There are some cases when the sum term in (4) is the same (or very close) for the different rolls. If this is the case, when adding amplitudes from several rolls, the Bessel functions of different  $r_{0,m}$  (and different  $n$ ) are added, and give an interlayer modulation (IM), typically of period  $2/c$  (inverse of the interlayer distance). (Note that the apparent period of the IM on the diagram varies with the same coefficient  $\alpha$  as the RDM, supposing that  $\alpha$  is about equal for different rolls.)

This is closely true at 000 ( $l$  and  $n = 0$ ), and it is the origin of the 002i reflections. For reflections  $\neq 000$ , it may also be true, if atoms follow specific pilings of the layers. Especially, if atoms of different rolls are at same altitude  $z_j$  (if  $z_j$  is independent of  $m$ ), IM appear in the diffracted pattern along  $z$ -axis (where  $n = 0$ ). (The number of atoms in the true cell, only slightly differs between rolls.) (This case will appear in Sect. 4.3.3.) The case where atoms of different rolls are at same angle  $\phi_j$  (if  $\phi_j$  is independent of  $m$ ) is not symmetrical. IM may not appear along  $r$ -axis (where  $l = 0$ ) because  $n$  is a function of  $m$ . In addition, such structure is not compatible with same helicity for the rolls.

Some IM appeared in the numerical simulation of [16] were a homo-helical layer piling also respects a rotational symmetry around  $z$ -axis. This was done for pilings such that atoms of different rolls are at same altitude  $z_j$  every roll, or every two rolls, giving modulations of respectively  $2c^*$ , and  $c^*$  in the reciprocal space [17].

For a MWNT, RDM can only be observed clearly, if one helicity corresponds to one diameter, or to a narrow dispersion of diameters. Otherwise, RDM from different diameters interfere in the pattern.

#### 4.1.4 Modulations in the pattern of a bundle of MWNT

A bundle of MWNT is a combination of the two previous cases. The diffracted amplitude of one roll  $m$  at one reflection is:

$$F_n^m(R, l) \sim \exp[ir_m R] \exp \left[ in \left( \frac{\pi}{2} \right) \right] J_n(2\pi r_{0,m} R) \times \sum_{j_m} f_{j_m} \exp \left[ i \left( n(\phi_{j_m}) + 2\pi \frac{l(z_{j_m})}{C} \right) \right]. \quad (5)$$

The total amplitude at one reflection is found by summing such terms for each roll contributing. (All rolls for the 000 reflection, and only rolls of a given helicity for

other reflections.) Unlike previous case of a MWNT, here, many rolls are interfering, and among which many have same diameter. The sum is more conveniently grouped by diameters:

$$F_n(R, l) \sim \sum_{\text{diameters}} J_n(2\pi r_{0,m} R) \times \sum_{\substack{\text{bundle} \\ \text{lattice}}} \exp[ir_m R] \exp \left[ in \left( \frac{\pi}{2} \right) \right] \times \sum_{j_m} f_{j_m} \exp \left[ i \left( n(\phi_{j_m}) + 2\pi \frac{l(z_{j_m})}{C} \right) \right]. \quad (6)$$

BLM can only be observed near 000 ( $n$  and  $l = 0$ ), if the bundle is thick, if the lattice is regular, and if MWNT are closely identical. (Else, the bundle lattice is different for each diameter.) RDM will appear if one reflection corresponds to only one diameter (or to a narrow dispersion of diameters). The number of rolls interfering reinforces its intensity on average. The IM will appear at 000 ( $n$  and  $l = 0$ ) as 002i reflections, and on  $z$ -axis ( $n = 0$ ), if atoms have same altitude  $z_j$  for all rolls in each MWNT (as in Sect. 4.1.3). (The altitudes of the MWNT inside the bundle do not need to be correlated.) In this case, lattice term has about same value for all diameters.

## 4.2 Experimental procedure and technical difficulties

All diagrams were obtained with the Hitachi HF-3000 TEM, equipped with a FEG gun. Comparable diagrams could not be obtained using a thermal emission gun microscope, showing that the high coherency of the illumination source is essential to resolve fine modulations in the pattern.

The main draw back to diffraction on a fibre is the weakness of the pattern. Indeed, the diffracting surface is very small, compared to the total irradiated surface. This problem is critical for tubes with few atomic layers. In order to enhance the diffracted signal, it is better to use the largest selected area aperture (although this increases the ratio non-diffracted/diffracted intensity) and to select a very long exposure time (typically, several minutes with the FEG). The tube should ideally be on a diameter of the aperture. Most often, the diffraction pattern is so weak that it is not observable on screen when taking the photo.

In the product, zones favourable to tube diffraction are few. Ideally, the diffracting tube should be well away from the rest of the material to avoid undesirable patterns. (Diffracting area does not strictly correspond to selected area, because of spherical aberration.) Also, the observed fibre should be perpendicular to the beam and as strait as possible. A fibre curved in the observation plane or twisted around its axis (common for bundles) leads to a distorted diffraction pattern with arcs instead of lines. Unfortunately, tubes best suited for diffraction are often not well suited for imaging. This is because parts of the tube that are away from the rest of the material

(good for diffraction), suffer more electron charging (bad for imaging).

### 4.3 Patterns observed from tubes and bundles (See Figs. 3–5)

#### 4.3.1 Main reflections and distribution of helicities

Because of the drastic observation conditions, a limited number of diagrams could be obtained. 15 nanotubes or thin bundles could be observed with at least one helicity, one of which was a large MWNT (Fig. 4). (Not all diagrams enabled fine modulation observation.) Non-chiral helicities were clearly dominant, but unlike other reports [18,19], we do not observe dominance of armchair or zigzag type. Among 15 fibres observed, 10 featured zigzag helicity, 8 featured armchair helicity, 3 featured both, 2 featured chiral helicity (Figs. 4, 6). The large MWNT (Fig. 4) contained an exceptionally high number of helicities, while thin tubes contained a unique or a narrow dispersion of helicity. This tends to say that tubes maintain an orientation in piling on a short order, but can not do so on long order. Also, it is remarkable that one (or few) helicity is also prevalent in a bundle (Figs. 3, 5). This supports the idea that tubes are not assembled together after their respective growth, but grow influencing each other. All diffraction patterns obtained showed the 002i reflections (sometime weak), indicating some degree of multi-layering.

#### 4.3.2 Roll diameter modulations (RDM)

Modulations expected from Section 4.1 are summarised in Table 1. For a MWNT bundle, RDM may be extinct because rolls of different diameter share same helicity and hence interfere. However, RDM may still appear, firstly because we are mostly looking at thin tubes with few different diameters, and secondly because a bundle may contain a large number of rolls for a given diameter. In Figure 3 which results from a large MWNT bundle, a RDM is observed on the 110 circle (right arrow) at 1.9 nm. (RDM measurement is corrected from the  $\alpha$  factor described in Sect. 4.1.1.) It is unsurprising to detect this diameter in the pattern, as it is a minimum inner diameter frequently observed by TEM. (See Sect. 3.2.) Another RDM is observed for the 110 circle, on  $r$ -axis (arrow). Fine pattern (left enlargement) actually shows a shift of the modulation (from 4.8 to 4.1 nm) with small angles to  $r$ -axis. We tentatively attribute this to a piling constraint causing a limited dispersion of roll diameters around 4.5 nm, as well as a limited dispersion of roll helicities around zigzag, and such that there is a (almost linear) relation between diameter and helicity for the constrained rolls. Diameters in range 4–5 nm could correspond to the outer diameter of a 4 or 5 layer tube with inner diameter near 2 nm. Such tubes are commonly observed by TEM. It may seem surprising that thinner rolls do not produce RDM when they are actually found in higher number by TEM imaging. However,

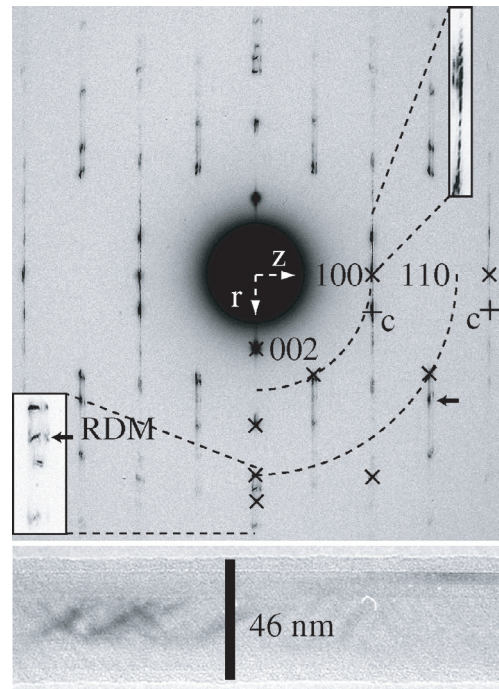


**Fig. 3.** Diffraction from a bundle of MWNT.  $\times$  signs indicate graphite indexes. 002i reflections, which indicate multi-layering, are found on  $r$ -axis. The spreading of the 004 inwards shows that inter-roll spacing is not constant and tends to be higher than graphite interlayer spacing. Reflections on the two dashed circles are the 100 and 110. Only zigzag type helicity is observed, however the angular dispersion (measurable on  $r$ -axis) is large enough ( $\pm 1^\circ$ ) to allow several helicities of low angles. (See left enlargement. Note that angular dispersion little affects the 006 reflection.) In addition, a dispersion of the orientations of the tubes in the bundle is shown by the relative thickness of lines when crossing  $z$ -axis. A RDM is clearly observed on  $r$ -axis at the 110 circle, with diameter in the range 4.1–4.8 nm, considering  $\alpha = 2.4$ . (RDM and IM periods are both measured taking in account the  $\alpha$  factor.) It is a favourable zone for this observation because rolls of different diameters are well segregated. The shape of this RDM (left enlargement) shows a correlation between roll diameter and helicity. A RDM corresponding to  $\sim 1.9$  nm ( $\alpha = 1.9$ ) is also observed (other arrow). Plus signs indicate IM of reflections (other than 000) on  $z$ -axis. It is very remarkable that they do not correspond to the  $c/2$  distance in real space, but to the  $c$  distance (0.67 nm, with  $\alpha = 1.1$ ). At 000 such long modulation is absent. This shows that in a (any) MWNT, atoms are on same altitudes  $z_i$ , every two rolls.

as all rolls are zigzag, or near zigzag, RDM of all rolls interfere. It may be that only largest and thinnest rolls RDM are favoured in such configuration. In Figure 5, the same 4.8 nm modulation is observed on the 110 circle, on  $r$ -axis. Another modulation of slightly different diameter is observed for the  $10^\circ$  helicity. It is worth wondering why such RDM appears most clearly at this position. One reason may be that pattern from slightly different helicities are best segregated near  $r$ -axis, away from 000. Another

**Table 1.** Fine modulations in the diffraction pattern as expected from theoretical considerations.

	RDM	BLM	IM
SWNT	Yes	No	No
Bundle of SWNT	Yes if regular	At 000 if regular	No
MWNT	Only if one helicity is associated with a small dispersion of diameters	No	Only at 000 and on $z$ -axis for specific pilings
Bundle of MWNT	Same as above but intensified by the number of iso-diameter rolls	At 000 if regular	Same as above

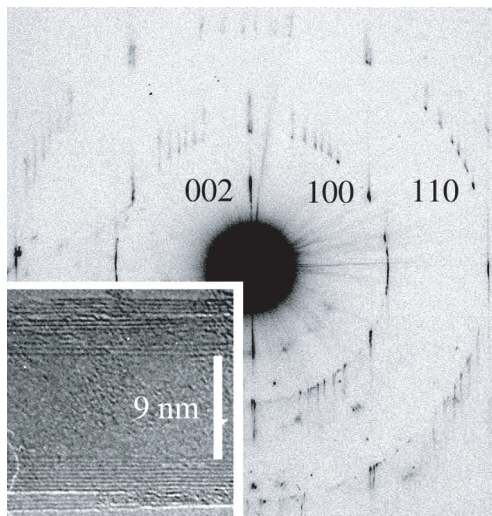


**Fig. 4.** Diffraction from large MWNT (possibly, two collateral MWNT). 002i reflections indicate multi-layering. Several helicities are present including zigzag and armchair type. Fine modulations are not clearly resolved, although some RDM seem present. (Some pollution reflections down image are caused by a boron particle near by.)

reason may be that the  $\alpha$  coefficient tends to segregate best modulations away from  $z$ -axis.

#### 4.3.3 Interlayer modulations (IM)

For a MWNT bundle, IM are expected only if specific pilings of the hexagonal layers occur. Such modulations indeed appeared for 5 of the 15 fibres observed (with same characteristics). All of these diagrams also indicated zigzag helicity. (One indicated both zigzag and armchair helicity.) A good instance is given in Figure 3 (modulations noted (c)). These modulations affect reflections along  $z$ -axis. They are not modulated by the  $c/2$  interlayer distance of real space as could be expected (apart from the obvious 000 reflection). Instead, they are modulated by a  $c$  interlayer distance of the real space.

This result is consistent with the specific piling described in Section 4.1.3 as well as with the simulation

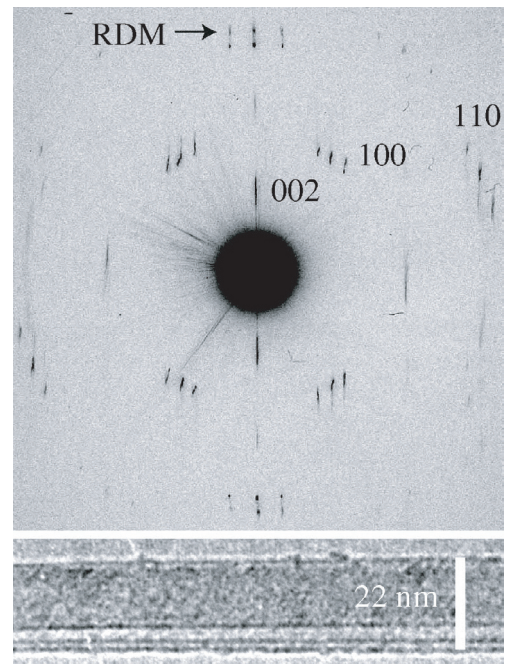


**Fig. 5.** Diffraction on a bundle of thin tubes. 002i reflections indicate multi-layering. Two helicities are present, zigzag type and a non-specific helicity near  $10^\circ$ . The same 4.8 nm RDM than for Figure 3 is observed on the 110 reflections near  $r$ -axis. (Arrow) (The tube is slightly tilted from the perpendicular of the beam, so that the diagram is expended horizontally.)

of [16] in which “initial stacking” (local stacking) is AB. Hence, a probable interpretation is that, in a (any) MWNT, atoms are on same altitudes  $z_i$  every two rolls, and the roll in between is shifted along  $z$ -axis (of a period non equal to  $C$ ) (it may also be rotated around  $z$ -axis). A grouping by neighbouring pairs of the hexagonal planes is consistent with the diatomic character of BN. However, in  $h$ -BN, hexagonal planes are simply superposed and form factor of B and N atoms are so close that 001 type reflections are not observable. Hence, this modulation is the sign of a constraint in MWNT layer piling.

A complete description of layer piling would require measuring the  $z$  shift between neighbouring layers, as well

as the relative angular position of the rolls. An eventual rotational symmetry around  $z$ -axis could be evidence by measurement of diffraction planes  $\Phi \neq 0$  in reciprocal space, as described in [16]. In any case, piling is not simply AB, because there is a misfit of periphery length between rolls. If the most inner roll is 1.9 nm large, the misfit of periphery between rolls is such that 3 hexagons on inner roll roughly superpose, with 4 hexagons on second roll and, five on third roll, ... The succession of rolls could therefore be such that roll number  $i$  is zigzag  $[24+8(i-1),0]$  and the rotational symmetry of the MWNT is 8.

Present piling may also be compared with that of very large BN MWNT characterised by high-resolution TEM imaging [20]. In this case a rhombohedral piling featured a similar  $z$ -shift between neighbouring zigzag rolls. However, this piling was found to be 3-roll periodic, which is different from the present 2-roll period result. A likely explanation is that such large MWNT (100 nm) are different from present thin tubes (<5 nm) in that they do not have a strong curvature constraint.

#### 4.3.4 Other modulations

BLM are not observed (at 000) for any of our MWNT bundle. This is unsurprising as present bundles are relatively thin, and as bundle lattices are probably irregular due to non-uniform number of layers in the tubes.

On the other hand, very short modulations that we attribute to the width of the bundle ( $\sim 46$  nm) are observable in Figure 3, right enlargement.

We would like to thank H. Hirayama, B. Jouffrey, K. Kimoto, A. Marraud, I. Massip, K.-I. Ohshima, C. Tsuruta, M. Uchida and for their support. We also thank L.C. Qin, P. Bernier, H. Biaisser, and O. Stéphan for useful discussions. The financial support was provided by the Ministry of Education, Science and Technology of Japan (Monbu-Kagakusho).

## References

1. A. Oberlin, M. Endo, *J. Cryst. Growth* **32**, 335 (1976)
2. E.A. Smith, *Powder Metall.* **14**, 27 (1971)
3. A. Lipp, K.A. Schwetz, K. Hunold, *J. Eur. Ceram. Soc.* **5**, 3 (1989)
4. T. Laude, Y. Matsui, A. Marraud, B. Jouffrey, *Appl. Phys. Lett.* **76**, 22 (2000)
5. T. Laude, Ph.D. thesis, University of Tsukuba and École Centrale Paris, March 2001 ([thomaslaude@yahoo.fr](mailto:thomaslaude@yahoo.fr) for a copy)
6. J.S. Speck, M. Endo, M.S. Dresselhaus, *J. Cryst. Growth* **94**, 834 (1989)
7. S. Iijima, *Nature* **354**, 56 (1991)
8. X.F. Zhang et al., *J. Cryst. Growth* **130**, 368 (1993)
9. L.C. Din et al., *Chem. Phys. Lett.* **268**, 101 (1997)
10. L.C. Qin, *J. Mater. Res.* **9**, 9 (1994)
11. A. Lucas, V. Bruyninckx, P. Lambin, *Europhys. Lett.* **35**, 355 (1996)
12. P. Lambin, A. Lucas, *Phys. Rev. B* **56**, 3571 (1997)
13. S. Iijima, T. Ichihashi, *Nature* **363**, 603 (1993)
14. L. Henrard, A. loiseau, C. Journet, P. Bernier, *Eur. Phys. J. B* **13**, 661 (2000)
15. J.-F. Colomer, L. Henrard, Ph. Lambin, G. Van Tenderloo, *Eur. Phys. J. B* **27**, 111 (2002)
16. S. Amelinckx, A. Lucas, P. Lambin, *Rep. Prog. Phys.* **62**, 1471 (1999)
17. Other articles related to IM modulation were published during editorial process of present article: Kociak et al., *Phys. Rev. Lett.* **89**, 15 (2002); Kociak et al., *Eur. Phys. J. B* **32**, 405 (2003); J.-F. Colomer et al., *Nano Lett.* **3**, 685 (2003)
18. X. Blase, A. De Vita, J.-C. Charlier, R. Car, *Phys. Rev. Lett.* **80**, 1666 (1998)
19. R.S. Lee et al., *Phys. Rev. B* **64**, 121405(R) (2001)
20. L. Bourgeois, Y. Bando, T. Sato, *J. Phys. D* **33**, 1902 (2000)